RESEARCH ARTICLE | OCTOBER 03 2012

Reconstructing acoustic obstacles by planar and cylindrical waves

Jingzhi Li; Hongyu Liu; Hongpeng Sun; Jun Zou

J. Math. Phys. 53, 103705 (2012)
https://doi.org/10.1063/1.4751282

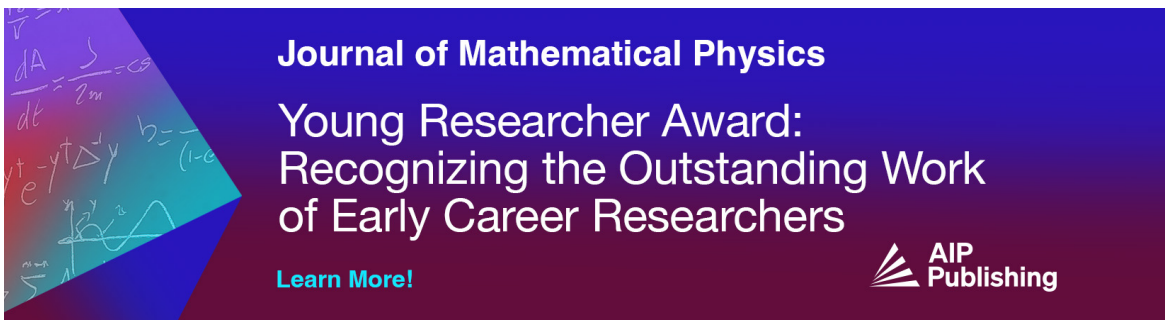

Reconstructing acoustic obstacles by planar and cylindrical waves

Jingzhi Li,[1,a)] Hongyu Liu,[2,b)] Hongpeng Sun,[3,c)] and Jun Zou[4,d)]
[1]*Department of Financial Mathematics and Engineering, South University of Science and Technology, Shenzhen 518055, People's Republic of China*
[2]*Department of Mathematics and Statistics, University of North Carolina at Charlotte, North Carolina 28223, USA and School of Mathematics and Statistics, Central South University, Changsha, Hunan 410075, People's Republic of China*
[3]*Institute of Mathematics, Academy of Mathematics and Systems Science, Chinese Academy of Sciences, Beijing 100190, People's Republic of China*
[4]*Department of Mathematics, The Chinese University of Hong Kong, Shatin, Hong Kong*

(Received 25 April 2012; accepted 22 August 2012; published online 3 October 2012)

In this paper, we develop a novel method of reconstructing acoustic obstacles in $\mathbb{R}^2$, which follows a similar spirit of the linear sampling method originated by Colton and Kirsch. The reconstruction scheme makes use of the near-field measurements encoded into the boundary Dirichlet-to-Neumann map or the Neumann-to-Dirichlet map. Both the plane waves and cylindrical waves are shown to meet the reconstruction purpose. Rigorous mathematical justification of the reconstruction scheme is established. The mapping properties of the newly introduced function operators involved in the reconstruction scheme are established. These results are of significant mathematical interests for their own sake. Moreover, due to the distinct properties of the function operators, the indictor function in the proposed reconstruction scheme exhibits completely different behaviors from those having been established for the indictor function in the original linear sampling method for inverse scattering problems. Numerical experiments are presented to illustrate the effectiveness of the proposed reconstruction scheme. © *2012 American Institute of Physics*. [http://dx.doi.org/10.1063/1.4751282]

I. INTRODUCTION

This work is concerned with the inverse problem of imaging obstacles located in the homogeneous space by acoustic wave measurements. Consider an impenetrable scatterer D, which is assumed to be the open complement of an unbounded domain of C^2 class in $\mathbb{R}^2$. The scatterer is allowed to have more than one (but finitely many) obstacle component. The time-harmonic wave propagation in $\mathbb{R}^2\backslash\bar{D}$ is governed by the celebrated Helmholtz equation

$$(\Delta + k^2)u = 0 \quad \text{in} \quad \mathbb{R}^2\backslash\bar{D}, \tag{1}$$

where u represents the pressure of the wave. On the boundary ∂D of the obstacle, the wave exhibits various behaviors depending on the physical properties of the underlying obstacle. We have $u = 0$ on ∂D for a *sound-softD*, $\partial u/\partial \nu = 0$ on ∂D for a *sound-hard D*, and $\partial u/\partial \nu + i\lambda u = 0$ on ∂D for a scatterer D of *impedance type*. Here ν is the exterior unit normal to ∂D and $\lambda \in C^1(\partial D)$ is a positive function. We shall write

$$\mathcal{B}(u) = 0 \quad \text{on} \quad \partial D \tag{2}$$

a)li.jz@sustc.edu.cn.
b)hongyu.liuip@gmail.com.
c)hpsun@amss.ac.cn.
d)zou@math.cuhk.edu.hk.

for either of the aforementioned three boundary conditions or the mixed type. We would like to stress that the reconstruction method developed in the present paper is independent of the specific boundary condition. However, for the ease of exposition we stick mostly to Dirichlet or Neumann boundary conditions in our subsequent discussions.

In non-invasive probing, one intends to determine the target obstacle D by the knowledge of the waves away from the object. This inverse problem forms the basis of many areas of science and technology; see, e.g., Refs. 2, 7, 19, 28, and 29 and the references therein. There are two types of wave measurements that have been widely employed and investigated in the literature for this inverse problem: the scattering measurement encoded into the far-field pattern, and the boundary measurement encoded into the Dirichlet-to-Neumann (DtN) or Neumann-to-Dirichlet (NtD) map. Correspondingly, one would consider either the inverse scattering problem or the inverse boundary value problem. Many reconstruction schemes have been developed in different settings, among which we would like to mention two: the linear sampling method originated from Colton and Kirsch (see, e.g., Ref. 18) and the enclosure method due to Ikehata (see, e.g., Ref. 26, 27, and 25). These two schemes have received significant attention in the last decade due to their qualitative aspects. Particularly, these methods require no *a priori* knowledge of the underlying target obstacles. This is of essential importance from a practical viewpoint. There are many developments along this line; see, e.g., Refs. 6, 10, 14, 20–22, 24, 29–31, and 33–35 and the references therein.

In this paper, we are mainly interested in the inverse boundary value problem by using the boundary measurements for the reconstructing unknown obstacles. We would have more choices on the probing waves other than planar waves. To that end, we let Ω be an artificial domain containing D such that $\Omega\backslash\bar{D}$ is connected. It is assumed that Ω is of class C^2 and the origin belongs to Ω. For the Helmholtz equations (1) and (2) confined over $\Omega\backslash\bar{D}$, we impose the following boundary condition on the exterior boundary:

$$u = f \in H^{1/2}(\partial\Omega) \quad \text{on } \partial\Omega. \tag{3}$$

It is assumed that 0 is not an eigenvalue to the problems (1)–(3). Hence, we have a well-defined Dirichlet-to-Neumann map Λ_D defined as

$$\Lambda_D(f) = \left.\frac{\partial u}{\partial \nu}\right|_{\partial\Omega}, \tag{4}$$

where $u \in H^1(\Omega\backslash\bar{D})$ is the unique solution to (1)–(3) and ν denotes the exterior unit normal to $\partial\Omega$. The method we shall develop is to reconstruct D from the knowledge of Λ_D. Physically, f is the acoustic pressure injected on $\partial\Omega$, whereas $\Lambda_D(f)$ is the corresponding acoustic flux measured on $\partial\Omega$. For our reconstruction scheme, the inputs could be either planar waves or cylindrical waves depending on a family of parameters $y \in \partial\widetilde{\Omega}$, where $\widetilde{\Omega}$ is a bounded domain in $\mathbb{R}^2$ that one could flexibly choose for practical purpose. We shall specify the probing waves in more details in the subsequent discussion. The crucial ingredient in our study is to introduce the following novel first kind integral equation:

$$\int_{\partial\widetilde{\Omega}} (\Lambda_D - \Lambda_0) u(x; y) g(y) ds(y) = \frac{\partial G(x, z)}{\partial \nu(x)}, \quad x \in \partial\Omega, \ z \in \Omega, \tag{5}$$

where $u(x; y)$ is a class of solutions to the Helmholtz equation (1) depending on the parameters $y \in \partial\widetilde{\Omega}$, Λ_0 stands for the DtN map without the inclusion D, and $G(x, z)$ is a Green's function for the Helmholtz equation in Ω with a vanishing Dirichlet boundary value on $\partial\Omega$. We shall show that the solution $g(y)$ to (5) exhibits different behaviors depending on whether z belongs to the interior or exterior of D. Therefore, we could make use of g as an indicator function to identify D. The idea of using an indicator function to recover the unknown obstacle has been essentially implemented in the linear sampling method originated in Ref. 18. As we mentioned earlier, there are a lot of developments along this line, but mostly based on far-field measurements corresponding to planar incident waves. There are relatively less studies based on the near-field data following the linear sampling spirit, and we refer to Ref. 17 for a near-field reconstruction method by using the Cauchy data and by combining the linear sampling method and the reciprocal gap functional, where under consideration is a Cauchy problem for acoustic scattering. In order to derive the indicating behaviors of the function g in (5),

we introduce some critical boundary operators and establish the corresponding mapping properties, which are of important mathematical interests for their own sake. Due to the distinct properties of the newly introduced boundary operators, the indictor function in the proposed reconstruction scheme exhibits completely different behaviors from those having been established for the indictor function in the linear sampling method for inverse scattering problems. Here, we would like to emphasize that one major distinction is that the boundary operator defining our method lacks the denseness property as that for the far-field operator defining the linear sampling method. It is also worthy noting that the DtN map has been widely adopted in various inverse problems. For example, in electric impedance tomography (EIT), the DtN map is the so-called current-to-flux map (see, e.g., Refs. 8, 36, and 37 for comprehensive surveys), and our method developed in the current work could be modified to the reconstruction of the supports of electric inclusions from current-to-flux measurements. However, the EIT problem is harder due to its strong instability, and we refer to Ref. 5 and the references therein for some interesting results on this topic. The DtN map is also used in a very different manner in the obstacle reconstructions associated with different inverse problems, for instance, in the enclosure method,[25–27,33] where the sources are generated by the more complicated complex geometric optics (CGO) waves.

Alternatively, our method works also with the Neumann-to-Dirichlet map. Actually, for the Helmholtz equations (1) and (2) confined over $\Omega\backslash\bar{D}$, one imposes the following boundary condition on the exterior boundary:

$$\frac{\partial u}{\partial \nu} = f \in H^{-1/2}(\partial\Omega) \quad \text{on } \partial\Omega. \tag{6}$$

Again we assume that 0 is not an eigenvalue to the problems (1)–(3), then the NtD map Υ_D is defined by

$$\Upsilon_D(f) = u|_{\partial\Omega}, \tag{7}$$

where $u \in H^1(\Omega\backslash\bar{D})$ is the unique solution to (1), (2), and (6). The counterpart to (5) is given by

$$\int_{\partial\widetilde{\Omega}} (\Upsilon_D - \Upsilon_0) u(x; y) g(y) ds(y) = G_N(x, z), \quad x \in \partial\Omega, \ z \in \Omega, \tag{8}$$

where Υ_0 is the NtD map without the inclusion D, and $G_N(x, z)$ is a Green's function for the Helmholtz equation on Ω with a vanishing Neumann boundary value on $\partial\Omega$.

The rest of the paper is organized as follows. We develop our reconstruction method based on the DtN map in Sec. II, and show how to modify the reconstruction scheme for the NtD map in Sec. III. Section IV is devoted to the derivation of the explicit forms of Green's functions implemented in our method when Ω is a disk. We shall conduct extensive numerical experiments to illustrate the effectiveness of the proposed method in Sec. V, and conclude the work in Sec. VI.

II. RECONSTRUCTION BY THE DtN MAP

In this section, we develop our reconstruction scheme based on the DtN map using the near-field flux measurements. The discussion will be concurrent for both plane waves and cylindrical waves. We start with the plane wave of the form:

$$w(x, y) = e^{ikx\cdot y}, \quad x \in \mathbb{R}^2, \ y \in \mathbb{S}^1, \tag{9}$$

where $\mathbb{S}^1$ is the unit circle in $\mathbb{R}^2$, and its corresponding (planar) Herglotz wave function

$$(Hg)(x) := w_g(x) = \int_{\mathbb{S}^1} e^{ikx\cdot y} g(y) ds(y), \quad x \in \mathbb{R}^2, \tag{10}$$

where $g(y) \in L^2(\mathbb{S}^1)$. We also define

$$U_p := \left\{ w_g(x) \mid w_g(x) = \int_{\mathbb{S}^1} e^{ikx\cdot y} g(y) ds(y), \ g(y) \in L^2(\mathbb{S}^1) \right\}. \tag{11}$$

In two dimensions, the cylindrical waves (cf. Refs. 12 and 13) are of the form

$$w(x, y) = J_n(k|x - y|)e^{in\hat{\phi}}, \quad x \in \mathbb{R}^2, \quad n \in \mathbb{Z}, \tag{12}$$

where $J_n(t)$, $t \in \mathbb{R}$ is the nth order Bessel function, and in polar coordinates, $y = |y|e^{i\phi'} \in \partial\Omega$, $x = |x|e^{i\phi} \in \mathbb{R}^2$, $x - y = |x - y|e^{i\hat{\phi}}$. We shall make use of the plane wave (9) or the cylindrical wave (12) as the probing input for our reconstruction scheme; namely, in (3) and (6), f and g would be $w(x, y)|_{\partial\Omega}$ and $\frac{\partial w(x,y)}{\partial \nu}|_{\partial\Omega}$, respectively, with w being given either in (9) or in (12). It is noted that according to our earlier notation, the parameter set $\partial\widetilde{\Omega}$ would be $\mathbb{S}^1$ for the plane waves and $\partial\Omega$ for the cylindrical waves, and this should be clear in the context of our subsequent study. Define the Bessel-Herglotz wave function as follows:

$$(Bg)(x) := w_g(x) = \int_{\partial\Omega} J_n(k|x - y|)e^{in\hat{\phi}}g(y)ds(y), \quad x \in \mathbb{R}^2, \tag{13}$$

where $g(y) \in L^2(\partial\Omega)$. Similar to (11), we introduce

$$U_b := \left\{ w_g(x) \mid w_g(x) = \int_{\partial\Omega} J_n(k|x - y|)e^{in\hat{\phi}}g(y)ds(y), \ g(y) \in L^2(\partial\Omega) \right\}. \tag{14}$$

In light of the linear superposition of the Helmholtz system, we establish another pair of solutions to the Helmholtz equation.

Lemma 2.1: Let $u(x; y) \in H^1(\Omega\backslash\bar{D})$ be the solution to the Helmholtz equations (1)–(3) associated with the Dirichlet boundary value $f(x, y) = w(x, y)|_{\partial\Omega}$ with $w(x, y) = e^{ikx\cdot y}$ or $w(x, y) = J_n(k|x - y|)e^{in\hat{\phi}}$, $y \in \partial\widetilde{\Omega}$. Let w_g be a Herglotz wave function (planar or Bessel, resp.). Then the solution to

$$\begin{cases} (\Delta + k^2)u = 0 \ \text{ in } \ \Omega\backslash\bar{D}, \\ u|_{\partial D} = 0, \ \ u|_{\partial\Omega} = w_g|_{\partial\Omega}, \end{cases} \tag{15}$$

is given by

$$u_g(x) = \int_{\partial\widetilde{\Omega}} u(x; y)g(y)ds(y).$$

The proof of Lemma 2.1 follows directly from the well-posedness and linearity of the involved boundary value problems. We shall also need the following boundary value problem:

$$\begin{cases} (\Delta + k^2)v(x; y) = 0 \ \text{ in } \ \Omega\backslash\bar{D}, \\ v|_{\partial D} = -f(x, y), \ \ v|_{\partial\Omega} = 0. \end{cases} \tag{16}$$

It is easy to see that $v(x; y) = u(x; y) - w(x, y)$. Similarly to Lemma 2.1, we have

Lemma 2.2: Let $v(x; y) \in H^1(\Omega\backslash\bar{D})$ be the solution to the Helmholtz equation (16) associated with $f(x, y) = e^{ikx\cdot y}$ or $f(x, y) = J_n(k|x - y|)e^{in\hat{\phi}}$. Let w_g be a Herglotz wave function (planar or Bessel, resp.). Then the solution to

$$\begin{cases} (\Delta + k^2)v = 0 \ \text{ in } \ \Omega\backslash\bar{D}, \\ v|_{\partial D} = -w_g|_{\partial D}, \ \ v|_{\partial\Omega} = 0, \end{cases} \tag{17}$$

is given by

$$v_g(x) = \int_{\partial\widetilde{\Omega}} v(x; y)g(y)ds(y).$$

Since $v(x; y) = u(x; y) - w(x, y)$ in $\Omega\backslash\bar{D}$, we point out the following pivotal relation for our subsequent discussion:

$$\left.\frac{\partial v(x; y)}{\partial \nu(x)}\right|_{\partial\Omega} = \Lambda_D(f(x, y)) - \Lambda_0(f(x, y)). \tag{18}$$

Next, we introduce some function spaces:

$$H^1_\Delta(\Omega\backslash\bar{D}) := \{\, u \in H^1(\Omega\backslash\bar{D}) \;\mid\; (\Delta + k^2)u = 0 \text{ in } \Omega\backslash\bar{D} \text{ and } u|_{\partial\Omega} = 0 \,\},$$

$$H^{-1/2}_\Delta(\partial\Omega) := \left\{ \left.\frac{\partial u}{\partial \nu}\right|_{\partial\Omega} \;\mid\; u \in H^1_\Delta(\Omega\backslash\bar{D}) \right\},$$

where the boundary values $\frac{\partial u}{\partial \nu}|_{\partial\Omega}$ and $u|_{\partial\Omega}$ are all understood in the sense of traces. Clearly, $H^1_\Delta(\Omega\backslash\bar{D})$ and $H^{-1/2}_\Delta(\partial\Omega)$ are both Banach spaces. Define $S : L^2(\partial\widetilde{\Omega}) \to H^1_\Delta(\Omega\backslash\bar{D})$ by

$$Sg(x) := \int_{\partial\widetilde{\Omega}} v(x;y)g(y)ds(y) \tag{19}$$

and $L : L^2(\partial\widetilde{\Omega}) \to H^{-1/2}_\Delta(\partial\Omega)$ by

$$Lg(x) := \int_{\partial\widetilde{\Omega}} \frac{\partial v(x;y)}{\partial \nu(x)} g(y)ds(y). \tag{20}$$

By (17), we see $Sg(x)|_{\partial D} = -v_g(x)|_{\partial D}$ and $Sg(x)|_{\partial\Omega} = 0$. Also by the definitions of S and L we have $\left.\frac{\partial Sg}{\partial \nu}(x)\right|_{\partial\Omega} = Lg(x)$.

The following theorem plays a key role in the mathematical justification of our proposed reconstruction scheme.

Theorem 2.3: *$L : L^2(\partial\widetilde{\Omega}) \to H^{-1/2}_\Delta(\partial\Omega)$ is a compact linear operator. If k^2 is not a Dirichlet eigenvalue for $-\Delta$, respectively, in $\Omega\backslash\bar{D}$, Ω, and D, then L is injective and has a dense range in $H^{-1/2}_\Delta(\partial\Omega)$.*

Remark 2.4: We would like to emphasize that the boundary operator L only has dense range in $H^{-1/2}_\Delta(\partial\Omega)$, which is a subset of $H^{-1/2}(\partial\Omega)$. It is the lack of denseness in $H^{-1/2}(\partial\Omega)$ for the operator L that will result in some distinct indicating behaviors of the boundary density function g in (20) (see Theorem 2.6). On the other hand, we would like to note that the mapping properties in Theorem 2.3 are new in literature and of important mathematical interests for their own sake.

In order to prove Theorem 2.3, we shall need the following crucial lemma.

Lemma 2.5: With respect to the $H^{1/2}(\partial D)$-norm, the traces of (planar or Bessel-) Herglotz wave functions are dense in the space of the traces of the solutions to the Helmholtz equation on ∂D. Here, we impose the same assumption on k^2 as that in Theorem 2.3.

Proof: For the case with plane waves and the corresponding (planar) Herglotz wave functions, consider a solution $u \in H^1(D)$ to the Helmholtz equation $\Delta u + k^2 u = 0$ in D. By Theorem 7.3 in Ref. 29, for every $\varepsilon > 0$, there exists a Herglotz wave function w_g such that $\|w_g - u\|_{H^1(D)} \le \varepsilon$, which implies

$$\|w_g - u\|_{H^{1/2}(\partial D)} \le C_0 \|w_g - u\|_{H^1(D)} \le C_0 \varepsilon$$

for some positive constant C_0 by the trace theorem, thus proving the desired density.

We next consider the case with cylindrical waves and the corresponding Bessel-Herglotz wave functions. In fact, we shall show that $U_b|_{\partial\Omega}$ is dense in $H^{1/2}(\partial\Omega)$ and this implies U_b is dense in $\{u \in H^1(\Omega);\, (\Delta + k^2)u = 0\}$. In turn, $U_b|_{\partial D}$ is dense in the space of traces of the solutions to the Helmholtz equation on ∂D with respect to the $H^{1/2}(\partial D)$-norm. Clearly, it suffices to show that if $\varphi(x) \in H^{-1/2}(\partial\Omega)$ such that

$$\int_{\partial\Omega}\int_{\partial\Omega} J_n(k|x-y|)e^{ik\hat{\phi}} g(y)ds(y)\overline{\varphi(x)}ds(x) = 0, \quad \text{for } \forall g \in L^2(\partial\Omega), \tag{21}$$

then one must have $\varphi(x) = 0$. By (21), together with the use of Fubini's Theorem, we have

$$\int_{\partial\Omega} J_n(k|x-y|)e^{ik\hat{\phi}}\overline{\varphi(x)}ds(x) = 0. \tag{22}$$

Set

$$h(y) = \int_{\partial\Omega} J_n(k|x-y|)e^{ik\hat{\phi}}\overline{\varphi(x)}\,ds(x). \tag{23}$$

Clearly, $h(y)$ is an analytical function in $\mathbb{R}^2$ satisfying the Helmholtz equation. By (22), $h(y)|_{\partial\Omega} = 0$. These, together with our assumption that k^2 is not a Dirichlet eigenvalue for $-\Delta$ in Ω, imply that $h(y) = 0$ on Ω. By analytic continuation, we further see $h(y) = 0$ in $\mathbb{R}^2$. Next, we choose a sufficiently large central ball of radius $\tilde{R}$, denoted as $B(0, \tilde{R})$, such that $\Omega \Subset B(0, \tilde{R})$ and k^2 is not a Dirichlet eigenvalue for $-\Delta$ in $B(0, \tilde{R})$. We recall the following important expansion of Bessel function (see formula (D.3) in Appendix D of Ref. 15):

$$J_n(k|x-y|)e^{in\hat{\phi}} = \sum_{m=-\infty}^{\infty} J_{m-n}(k|y|)J_m(k|x|)e^{im\phi - i(m-n)\phi'}. \tag{24}$$

Plugging (24) into the integral representation (23) of $h(y)$, we have

$$h(y)|_{\partial B(0,\tilde{R})} = \sum_{m=-\infty}^{\infty} \int_{\partial\Omega} J_m(k|x|)e^{im\phi}\overline{\varphi(x)}ds(x)J_{m-n}(k|\tilde{R}|)e^{-i(m-n)\phi'}.$$

By virtue of $h(y)|_{\partial B(0,\tilde{R})} = 0$ and $J_{m-n}(k|\tilde{R}|) \neq 0$, $\forall m \in \mathbb{Z}$, together with the fact that the set $\{e^{-i(m-n)\phi'}, m \in \mathbb{Z}\}$ is a basis for $L^2(\partial B(0, \tilde{R}))$, we see

$$\int_{\partial\Omega} J_m(k|x|)e^{im\phi}\overline{\varphi(x)}ds(x) = 0, \quad \forall m \in \mathbb{Z}. \tag{25}$$

Next we shall make use of the following expansion of the Hankel function $H_0^{(1)}(k|x-y|)$ (cf. Refs. 15 and 19):

$$H_0^{(1)}(k|x-y|) = \sum_{m=-\infty}^{\infty} J_m(k|x|)H_m^{(1)}(k|y|)e^{im\phi'}e^{-im\phi}, \tag{26}$$

where $y \in \mathbb{R}^2\backslash B(0, \tilde{R})$ and $x \in \partial\Omega$. Multiplying $H_m^{(1)}(k|y|)e^{im\phi'}$ to the complex conjugate of Eq. (25) and summing up for all $m \in \mathbb{Z}$, together with the use of (26), we have by straightforward calculations:

$$H(y) := \int_{\partial\Omega} \Phi(k|y-x|)\varphi(x)ds(x) = 0 \text{ for } y \in \mathbb{R}^2\backslash B(0, \tilde{R}), \tag{27}$$

where $\Phi(k|y-x|) = i/4H_0^{(1)}(k|y-x|)$. By the mapping properties of single layer potential operator (cf. Ref. 32), we know that $H(y) \in H^1_{loc}(\mathbb{R}^2\backslash\partial\Omega)$ satisfying the Helmholtz equation. Moreover, $H(y)$ is analytic in $\mathbb{R}^2\backslash\bar{\Omega}$, and hence by continuation, we see $H(y) = 0$ in $\mathbb{R}^2\backslash\bar{\Omega}$. In the following, we denote by γ^+ and γ^- the one-sided trace operators for Ω and $\mathbb{R}^2\backslash\bar{\Omega}$. Again by the mapping properties of single layer potential operator, we have $\gamma^- H(y) = \gamma^+ H(y) = 0$ on $\partial\Omega$. Since $(\Delta + k^2)H(y) = 0$ on Ω, and by our assumption that k^2 is not a Dirichlet eigenvalue for $-\Delta$ in Ω, we see $H(y) = 0$ on Ω. Finally, by the jump properties of the single layer potential operator (cf. Ref. 32), we have

$$\varphi(x) = \gamma^+\frac{\partial H(y)}{\partial\nu} - \gamma^-\frac{\partial H(y)}{\partial\nu} \text{ on } \partial\Omega.$$

Hence $\varphi = 0$, which completes the proof. □

Proof of Theorem 2.3: We first prove the compactness of the operator L. In the sequel, $a \lesssim b$ means $a \leq Cb$ with C a generic constant that might change in different estimates but is fixed and finite in a single relation. By the classic regularity estimate for elliptic equations, we know for $g \in L^2(\partial\widetilde{\Omega})$, $Sg \in H^2(\Omega\backslash\bar{D})$. Hence,

$$\|Lg\|_{H^{1/2}(\partial\Omega)} = \|\partial Sg/\partial\nu\|_{H^{1/2}(\partial\Omega)} \lesssim \|Sg\|_{H^2(\Omega\backslash\bar{D})}. \tag{28}$$

Next, by the well-posedness of the system (17), we know $\|Sg\|_{H^2(\Omega\backslash\bar{D})} \lesssim \|w_g\|_{H^{3/2}(\partial D)}$. Hence,

$$\|Sg\|_{H^2(\Omega\backslash\bar{D})} \lesssim \|w_g\|_{H^{3/2}(\partial D)} \lesssim \|w_g\|_{H^2(D)} \lesssim \|g\|_{L^2(\partial\widetilde{\Omega})}. \tag{29}$$

By combining (28) and (29), we see

$$\|Lg\|_{H^{1/2}(\partial\Omega)} \lesssim \|g\|_{L^2(\partial\widetilde{\Omega})}.$$

That is, L maps $L^2(\partial\widetilde{\Omega})$ into $H^{1/2}(\partial\Omega)$ boundedly. Hence, L is compact.

Now we show the injectivity of L. Suppose $g \in L^2(\partial\widetilde{\Omega})$ and $Lg = 0$. Clearly, $Sg|_{\partial\Omega} = 0$ and $\frac{\partial Sg}{\partial\nu}|_{\partial\Omega} = Lg = 0$. Hence, by the unique continuation, we know $Sg = 0$ in $\Omega\backslash\bar{D}$. Therefore, $w_g|_{\partial D} = -Sg|_{\partial D} = 0$. Then, noting w_g is a solution for the Helmholtz equation in $H^1(D)$ and k^2 is not a Dirichlet eigenvalue, we see $w_g = 0$ in D. By unique continuation again, we see $w_g = 0$ in $\mathbb{R}^2$. If $w_g \in U_p$, then by Theorem 3.15 in Ref. 19, $g = 0$. If $w_g \in U_b$, we have

$$w_g(x) = \int_{\partial\Omega} J_n(k|x-y|)e^{in\hat{\phi}}g(y)ds(y) = 0 \ \text{ in } \ \mathbb{R}^2.$$

Then, by a completely similar argument to the second part of the proof for Lemma 2.5, we can show that $g = 0$.

Finally, we show that L has a dense range in $H_\Delta^{-1/2}(\partial\Omega)$. For every $\psi \in H_\Delta^{-1/2}(\partial\Omega)$, let $u \in H_\Delta^1(\Omega\backslash\bar{D})$ be such that $\frac{\partial u}{\partial\nu}|_{\partial\Omega} = \psi|_{\partial\Omega}$. Then by Lemma 2.5, there exists a (planar or Bessel) Herglotz wave function w_g such that for arbitrary small $\varepsilon > 0$, $\|w_g - u\|_{H^{1/2}(\partial D)} \le \varepsilon$. By the well-posedness of the boundary value problem (17), we see $\|Sg - u\|_{H^1(\Omega\backslash\bar{D})} \lesssim \varepsilon$. By the trace theorem, we further have $\|Lg - \psi\|_{H^{-1/2}(\partial\Omega)} \lesssim \|Sg - u\|_{H^1(\Omega\backslash\bar{D})} \lesssim \varepsilon$. This proves Theorem 2.3. □

For any $x \in \bar{\Omega}$ and $z \in \Omega$, let $G(x, z)$ be a Green's function associated with the Helmholtz equation with a vanishing Dirichlet value on $\partial\Omega$. For our reconstruction algorithm developed in the sequel, we take $G(x, z) = \Phi(x, z) - u(x, z)$, where $\Phi(x, z) = \frac{i}{4}H_0^{(1)}(k|x - z|)$ is the fundamental solution to the operator $-\Delta - k^2$ and $u(x, z)$ satisfies

$$(\Delta + k^2)u(x, z) = 0 \quad \text{in } \Omega, \quad u(x, z)|_{\partial\Omega} = \Phi(x, z)|_{\partial\Omega}, \tag{30}$$

for any fixed $z \in \Omega$. For the case with Ω being a central disk, an explicit form of $G(x, z)$ can be derived in the way demonstrated in Sec. IV. It is clear to see that $G(x, z) \in H_\Delta^1(\Omega\backslash\bar{D})$ if $z \in D$, which further implies $\frac{\partial G(x,z)}{\partial\nu(x)}|_{\partial\Omega} \in H_\Delta^{-1/2}(\partial\Omega)$ if $z \in D$.

Now we are ready to present the first main theorem and establish the reconstruction algorithm. To that end, we introduce the following crucial first kind integral equation for $g_z \in L^2(\partial\widetilde{\Omega})$:

$$(Lg_z)(x) = \frac{\partial G(x, z)}{\partial\nu(x)}, \quad x \in \partial\Omega, \ z \in \Omega, \tag{31}$$

which by (18) is equivalent to

$$\int_{\partial\widetilde{\Omega}} (\Lambda_D - \Lambda_0)(f(x, y))g_z(y)ds(y) = \frac{\partial G(x, z)}{\partial\nu(x)}, \quad x \in \partial\Omega, \ z \in \Omega\,. \tag{32}$$

Theorem 2.6: *For g_z in (31) or (32), we have*

(i) *If $z \in D$, then for every $\varepsilon > 0$, there exists $g_{z,\varepsilon} \in L^2(\partial\widetilde{\Omega})$ such that*

$$\|Lg_{z,\varepsilon}(x) - \frac{\partial G(x, z)}{\partial\nu(x)}\|_{H^{-1/2}(\partial\Omega)} \le \varepsilon. \tag{33}$$

Moreover, for every $z^* \in \partial D$ and every choice of $g_{z,\varepsilon} \in L^2(\partial\widetilde{\Omega})$ in (33),

$$\lim_{z\to z^*} \|g_{z,\varepsilon}\|_{L^2(\partial\widetilde{\Omega})} = \infty \ \text{ and } \ \lim_{z\to z^*} \|v_{g_{z,\varepsilon}}\|_{H^1(D)} = \infty. \tag{34}$$

(ii) *If $z \in \Omega\backslash\bar{D}$, we can solve (31) by the Tikhonov regularization to have a regularized solution $g_{z,\varepsilon}$ in $L^2(\partial\widetilde{\Omega})$, depending on a regularizer $\varepsilon > 0$. That is, $g_{z,\varepsilon}$ is the unique solution to the regularized system:*

$$\left(\varepsilon I + L^*L\right) g = L^* \frac{\partial G(\cdot, z)}{\partial\nu}\,. \tag{35}$$

Moreover, only one of the following two possibilities occurs to the sequence $\{g_{z,\varepsilon}\}$: *either there exists a sequence* $\varepsilon_n \to 0^+$ *such that*

$$\lim_{\varepsilon_n \to 0^+} \|Lg_{z,\varepsilon_n}(x) - \frac{\partial G(x,z)}{\partial \nu(x)}\|_{H^{-1/2}(\partial\Omega)} = 0, \tag{36}$$

and

$$\lim_{\varepsilon_n \to 0^+} \|g_{z,\varepsilon_n}\|_{L^2(\partial\widetilde{\Omega})} = \infty, \tag{37}$$

or, there exists a constant $C > 0$ *such that for all* $\varepsilon > 0$,

$$\|Lg_{z,\varepsilon}(x) - \frac{\partial G(x,z)}{\partial \nu(x)}\|_{H^{-1/2}(\partial\Omega)} \geq C. \tag{38}$$

Remark 2.7: Part (ii) of Theorem 2.6 tells that the following situation would not happen: there exists a sequence $\varepsilon_n \to 0^+$ *such that*

$$\lim_{\varepsilon_n \to 0^+} \|Lg_{z,\varepsilon_n}(x) - \frac{\partial G(x,z)}{\partial \nu(x)}\|_{H^{-1/2}(\partial\Omega)} = 0, \tag{39}$$

and

$$\liminf_{\varepsilon_n \to 0^+} \|g_{z,\varepsilon_n}\|_{L^2(\partial\widetilde{\Omega})} < \infty. \tag{40}$$

More precisely, we may interpret it as follows: for any point z *lying outside the obstacle, either the magnitude of its indicator function* g_{z,ε_n} *blows up, or the magnitude of the residual* $Lg_{z,\varepsilon_n} - \frac{\partial G(\cdot,z)}{\partial \nu(x)}$ *is bounded from below by a positive constant.*

Remark 2.8: By Theorem 2.6, we see that the norm of the function g_z *cannot completely determine whether a point lies inside or outside the obstacle* D, *especially for a point lying outside* D, *and one has to make further use of the indicating behaviors of the residual function* $Lg_z - \partial G(x,z)/\partial \nu$. *Since the Tikhonov regularization has been used, we know that the norms of* g_z *and* $Lg_z - \partial G(x,z)/\partial \nu$ *are related, but the indicating behaviors of* $Lg_z - \partial G(x,z)/\partial \nu$ *are due to the lack of denseness of the operator* L *as emphasized in Remark 2.4, and this can be seen from the following proof to Theorem 2.6.*

Proof of Theorem 2.6: We first verify (i). For $z \in D$, we obviously have $G(\cdot, z)|_{\partial D} \in H^{1/2}(\partial D)$. Hence by Lemma 2.5, for any $\varepsilon > 0$ there exists $g_{z,\varepsilon} \in L^2(\partial\widetilde{\Omega})$ such that

$$\|v_{g_{z,\varepsilon}} - G(\cdot, z)\|_{H^{1/2}(\partial D)} \leq \varepsilon\,. \tag{41}$$

In the rest of the proof, we let C denote a generic positive constant, which may differ at different estimates but is fixed and finite in a single relation. Since $v_{g_{z,\varepsilon}} = Sg_{z,\varepsilon}$ on ∂D and $G(\cdot, z) \in H^1_\Delta(\Omega\backslash\bar{D})$, by the well-posedness of problem (17) we have $\|Sg_{z,\varepsilon} - G(\cdot, z)\|_{H^1(\Omega\backslash\bar{D})} \leq C\varepsilon$. This, along with the trace theorem and the fact that $\partial Sg/\partial \nu = Lg$ on $\partial\Omega$, leads to the desired estimate (33).

We next show (34). By the trace theorem again,

$$\|Sg_{z,\varepsilon} - G(\cdot, z)\|_{H^{1/2}(\partial D)} \leq C\|Sg_{z,\varepsilon} - G(\cdot, z)\|_{H^1(\Omega\backslash\bar{D})}. \tag{42}$$

Assume contrarily that there exists $z^* \in \partial D$, $0 < M < \infty$ and a sequence $z_n \to z^*$ such that $\|v_n\|_{H^1(D)} \leq M$, where we write $v_n := v_{g_{z_n,\varepsilon}}$. Then by (41) we have

$$\|G(\cdot, z_n)\|_{H^{1/2}(\partial D)} \leq \|G(\cdot, z_n) - v_n\|_{H^{1/2}(\partial D)} + \|v_n\|_{H^{1/2}(\partial D)} \leq C(\varepsilon + M) \tag{43}$$

for all $n > 0$. However, noting that $G(\cdot, z)$ has the same singularity as the fundamental solution $\Phi(\cdot, z)$, we have $\|G(\cdot, z_n)\|_{H^1(U\backslash\bar{D})} \to \infty$ as $n \to \infty$ for any bounded region U containing D. This contradicts to (43), thus proves the second statement in (34). The first statement follows directly from the boundedness of the mapping $g \mapsto v_g|_D$ from $L^2(\partial\widetilde{\Omega})$ into $H^1(D)$.

Next, we demonstrate (ii). For a point $z \in \Omega\backslash D$ and small $\varepsilon > 0$, we introduce the Tikhonov functional $J_{z,\varepsilon} : L^2(\partial\widetilde{\Omega}) \to \mathbb{R}$ by

$$J_{z,\varepsilon}(g) = \|Lg - \frac{\partial G(\cdot, z)}{\partial \nu}\|^2_{H^{-1/2}(\partial\Omega)} + \varepsilon \|g\|^2_{L^2(\partial\widetilde{\Omega})}$$

for $g \in L^2(\partial\widetilde{\Omega})$. By the classical result on the regularities of solutions to (16) (cf. Ref. 23), we know the operator L has a continuous kernel and hence L^*L is compact from $L^2(\partial\widetilde{\Omega})$ to $L^2(\partial\widetilde{\Omega})$. Moreover, $L^*L + \varepsilon I$ is positive since L is injective by Theorem 2.3. Therefore, for any $\varepsilon > 0$, there exists a unique minimizer $g_{z,\varepsilon} \in L^2(\partial\widetilde{\Omega})$ to functional $J_{z,\varepsilon}$, which is given by (35). Now it suffices for us to show that (39) and (40) cannot hold simultaneously. Assume contrarily that both (39) and (40) are true, then we have a sequence $\{g_{z,\varepsilon_n}\}$ such that $\varepsilon_n \to 0^+$ as $n \to \infty$, and $\|g_{z,\varepsilon_n}\|_{L^2(\partial\widetilde{\Omega})} \le C$ for all n and (39) also holds. Then there exists a subsequence $g_{z,\varepsilon_{n'}}$ which converges weakly to some $g \in L^2(\partial\widetilde{\Omega})$. By the compactness of L, we have $Lg_{z,\varepsilon_{n'}} \to Lg$ in $H^{-1/2}_{\Delta}(\partial\Omega)$, which implies $Lg(x) = \frac{\partial G(x,z)}{\partial \nu(x)}|_{\partial\Omega}$ by means of (39). Therefore, we obtain $\frac{\partial Sg}{\partial \nu} = Lg$ and $Sg(x) = G(x, y)$ on $\partial\Omega$. Using Holmgren's uniqueness theorem, we see $Sg(x) = G(x, z)$ in a neighborhood of $\partial\Omega$. By the unique continuation principle, we further have $Sg(x) = G(x, z)$ in $\Omega\backslash(\bar{D} \bigcup \{z\})$. However, this is impossible, since $Sg(x) \in H^1(\Omega\backslash\bar{D}) \cup H^1(\Omega\backslash(\bar{D} \bigcup \{z\})$, but $G(x, z)$ does not belong to $H^1(\Omega\backslash(\bar{D} \bigcup \{z\})$ for $z \in \Omega\backslash D$. This proves (ii), hence completes the proof of Theorem 2.6. □

Theorem 2.6 suggests a procedure to determine if a point $z \in \Omega$ lies in D or not. To do so, we may choose two cut-off values $c_1, c_2 > 0$. Then one can first find a Tikhonov regularized solution $g_{z,\varepsilon}$ to (31). If $\|g_{z,\varepsilon}\|_{L^2(\partial\widetilde{\Omega})} > c_1$, we count $z \notin D$; otherwise we further compute the residual $Lg_{z,\varepsilon} - \partial G(\cdot, z)/\partial \nu$. If the norm of this residual is less than c_2, we count $z \in D$, or $z \notin D$ otherwise.

The above discussion leads us to the following numerical reconstruction scheme.

A. Numerical reconstruction scheme (DtN)

Select two cut-off values $c_1, c_2 > 0$.

Step 1. Collect the measurement data $\frac{\partial u(x;y)}{\partial \nu}$ on $\partial\Omega$ corresponding to the excitation $f(x, y)$ on $\partial\Omega$ for different y's .
Step 2. Select a sampling mesh $\mathcal{T}_h$ over the domain Ω.
Step 3. For each sampling mesh point $z \in \mathcal{T}_h$, compute a Tikhonov regularized solution $g_{z,\varepsilon}$ to (31).
Step 4. If $\|g_{z,\varepsilon}\|_{L^2(\partial\widetilde{\Omega})} > c_1$, we count $z \notin D$; otherwise we compute the residual $Lg_{z,\varepsilon} - \partial G(\cdot, z)/\partial \nu$. If the norm of this residual is less than c_2, we count $z \in D$; otherwise we count $z \notin D$.

III. RECONSTRUCTION BY THE NtD MAP

We proposed a reconstruction scheme of an unknown obstacle in Sec. II A by the DtN map. Similar ideas work as well for the NtD map. In this section, we present some necessary modifications for the case with the NtD map. Let $u(x; y) \in H^1(\Omega\backslash\bar{D})$ be the unique solution to the system:

$$\begin{cases} (\Delta + k^2)u(x; y) = 0 \ \text{ in } \Omega\backslash\bar{D}, \\ u = 0 \text{ on } \partial D; \quad \partial u/\partial \nu = \partial w(\cdot, y)/\partial \nu \text{ on } \partial\Omega, \end{cases} \tag{44}$$

where $w(x, y)$ is the (planar or cylindrical) incident wave as introduced in Sec. II. Here it is assumed that k^2 is not a Neumann eigenvalue to $-\Delta$ in Ω and 0 is not an eigenvalue to the problem (44). We also set $v(x; y) = u(x; y) - w(x, y)$, then $v(x; y)$ satisfies

$$\begin{cases} (\Delta + k^2)v(x; y) = 0 \ \text{ in } \Omega\backslash\bar{D}, \\ v = -w(x, y) \text{ on } \partial D; \quad \partial v/\partial \nu = 0 \text{ on } \partial\Omega. \end{cases} \tag{45}$$

The NtD map associated with (44) is given by

$$\Upsilon_D\left(\frac{\partial w(x,y)}{\partial \nu}\Big|_{\partial\Omega}\right) = u(x;y)|_{\partial\Omega}.$$

When the inclusion D is empty, we shall write Υ_D as Υ_0.

Similarly to Lemmas 2.1 and 2.2, we have the following result by linear superposition.

Proposition 3.1: Let $u(x;y)$ and $v(x;y) \in H^1(\Omega\backslash\bar{D})$ be the solution to (44) and (45), *respectively, associated with $w(x,y)$, and w_g be a Herglotz wave function (planar and Bessel resp.). Then the solutions to the system:*

$$\begin{cases}(\Delta + k^2)u(x;y) = 0 \ \text{ in } \ \Omega\backslash\bar{D},\\ u|_{\partial D} = 0, \ \ \frac{\partial u}{\partial \nu}|_{\partial\Omega} = \frac{\partial w_g}{\partial \nu}|_{\partial\Omega}\end{cases} \tag{46}$$

and

$$\begin{cases}(\Delta + k^2)v(x;y) = 0 \ \text{ in } \Omega\backslash\bar{D},\\ v|_{\partial D} = -w_g|_{\partial D}, \ \ \frac{\partial v}{\partial \nu}|_{\partial\Omega} = 0\end{cases} \tag{47}$$

are, respectively, given by

$$u_g(x) = \int_{\partial\widetilde{\Omega}} u(x;y)g(y)ds(y) \quad \text{and} \quad v_g(x) = \int_{\partial\widetilde{\Omega}} v(x;y)g(y)ds(y)\,.$$

For the subsequent analysis, we introduce the following function spaces:

$$\hat{H}^1_\Delta(\Omega\backslash\bar{D}) := \{\, u \in H^1(\Omega\backslash\bar{D}),\ (\Delta + k^2)u = 0 \text{ in } \Omega\backslash\bar{D} \text{ and } \frac{\partial u}{\partial \nu}|_{\partial\Omega} = 0\,\},$$

$$\hat{H}^{1/2}_\Delta(\partial\Omega) := \{\, u|_{\partial\Omega};\ u \in \hat{H}^1_\Delta(\Omega\backslash\bar{D})\,\}$$

and the operator $\hat{S} : L^2(\partial\widetilde{\Omega}) \to \hat{H}^{1/2}_\Delta(\partial\Omega)$ defined by

$$\hat{S}g(x) := v_g(x)|_{\partial\Omega} = \int_{\partial\widetilde{\Omega}} v(x;y)g(y)ds(y)|_{\partial\Omega}, \tag{48}$$

where $v_g(x)$ is the solution to (47). Similarly to Theorem 2.3, we have

Theorem 3.2: *The operator $\hat{S} : L^2(\partial\widetilde{\Omega}) \to \hat{H}^{1/2}_\Delta(\partial\Omega)$ is compact and has a dense range. Furthermore, $\hat{S}$ is injective provided that k^2 is not a Dirichlet eigenvalue to $-\Delta$ in D and Ω.*

Let $G_N(x,z)$, $x \in \bar{\Omega}$, $z \in \Omega$, be a Green's function for the Helmholtz equation with a homogeneous Neumann condition on $\partial\Omega$. For the convenience, we will take $G_N(x,z) = \Phi(x,z) - u(x,z)$, where $\Phi(x,z)$ is the fundamental solution to $-\Delta - k^2$ for any fixed z, and $u(x,z)$ satisfies

$$(\Delta + k^2)u(x,z) = 0 \quad \text{in } \Omega, \qquad \frac{u(x,z)}{\partial \nu} = \frac{\partial \Phi(x,z)}{\partial \nu} \text{ on } \partial\Omega \tag{49}$$

for any fixed $z \in \Omega$. When Ω is a simple disk, we will derive the explicit expression of $G_N(x,z)$ in Sec. IV.

Now we are ready to present a major theorem of this section, a counterpart to Theorem 2.6 based on the NtD map; and its proof follows the one of Theorem 2.6, with slight modifications. The governing equation involved in the theorem is now given by

$$\hat{S}g_z(x) = G_N(x,z), \ \ x \in \partial\Omega, \ z \in \Omega, \tag{50}$$

or equivalently,

$$\int_{\partial\widetilde{\Omega}} (\Upsilon_D - \Upsilon_0)\Big(\frac{\partial w(x,y)}{\partial \nu}\Big|_{\partial\Omega}\Big)g_z(y)ds(y) = G_N(x,z), \ \ x \in \partial\Omega, \ z \in \Omega.$$

Theorem 3.3: *For g^z* in (50), *we have*

(i) *If $z \in D$, then for every $\varepsilon > 0$ there exists $g_{z,\varepsilon}$ to (50) such that*

$$\|\hat{S} g_{z,\varepsilon}(x) - G_N(x, z)\|_{H^{1/2}(\partial\Omega)} \leq \varepsilon. \tag{51}$$

Moreover, for every $z^* \in \partial D$ and every choice of $g_{z,\varepsilon} \in L^2(\partial\widetilde{\Omega})$ in (51),

$$\lim_{z \to z^*} \|g_{z,\varepsilon}\|_{L^2(\partial\widetilde{\Omega})} = \infty \text{ and } \lim_{z \to z^*} \|v_{g_{z,\varepsilon}}\|_{H^1(D)} = \infty. \tag{52}$$

(ii) *If $z \in \Omega \backslash \bar{D}$, we can solve (50) by the Tikhonov regularization to have a regularized solution $g_{z,\varepsilon}$ in $L^2(\partial\widetilde{\Omega})$, depending on a regularizer ε. That is, $g_{z,\varepsilon}$ is the unique solution to the system:*

$$(\varepsilon I + \hat{S}^* \hat{S}) g = \hat{S}^* G_N(\cdot, z). \tag{53}$$

Moreover, only one of the following two possibilities occurs to the sequence $\{g_{z,\varepsilon}\}$: either there exists a sequence $\varepsilon_n \to 0^+$ such that

$$\lim_{\varepsilon_n \to 0^+} \|\hat{S} g_{z,\varepsilon_n}(x) - G_N(x, z)\|_{H^{1/2}(\partial\Omega)} = 0 \tag{54}$$

and

$$\lim_{\varepsilon_n \to 0^+} \|g_{z,\varepsilon_n}\|_{L^2(\partial\widetilde{\Omega})} = \infty, \tag{55}$$

or, there exists a positive constant C such that for all $\varepsilon > 0$,

$$\|\hat{S} g_{z,\varepsilon}(x) - G_N(x, z)\|_{H^{1/2}(\partial\Omega)} \geq C. \tag{56}$$

Similarly to our discussion in Sec. II A for the motivation of the numerical reconstruction scheme (DtN) by Theorem 2.6, Theorem 3.3 above suggests us the following reconstruction scheme by using the NtD map.

A. Numerical reconstruction scheme (NtD)

Select two cut-off values $c_1, c_2 > 0$.

Step 1. Collect the measurement data $u(x; y)$ on $\partial\Omega$ corresponding to $\partial w(x, y)/\partial\nu$ on $\partial\Omega$ for different y's.

Step 2. Select a sampling mesh $\mathcal{T}_h$ over the domain Ω.

Step 3. For each sampling point $z \in \mathcal{T}_h$, compute a Tikohnov regularized solution $g_{z,\varepsilon}$ to Eq. (50).

Step 4. If $\|g_{z,\varepsilon}\|_{L^2(\partial\widetilde{\Omega})} > c_1$, we count $z \notin D$; otherwise we compute the residual $\hat{S} g_{z,\varepsilon_n}(x) - G_N(x, z)$. If the norm of this residual is less than c_2, we count $z \in D$; otherwise we count $z \notin D$.

Remark 3.4: If the boundary condition of the obstacle is of general type (2), all the results we have obtained in Secs. II and III still hold. In particular, we can show similar density for the Herglotz wave functions (U_p or U_b) in $H^1(\Omega)$ and similar results to Theorems 2.6 and 3.3.

IV. GREEN'S FUNCTIONS

In our reconstruction schemes developed in Secs. II, III the Green's functions $G(x, z)$ and $G_N(x, z)$ are needed. It is noted that G and G_N can be obtained by solving the Helmholtz equations (30) and (49), respectively. Clearly, they do not depend on the unknown obstacle D and can be computed in advance before one starts the reconstruction process. Particularly, when Ω is a central disk of radius R, one could derive the explicit forms of those Green's functions. For this case, it is worthy noting that due to the positive wave number k, the so-called *method of image* or *reflection* does not

work to construct the Green's functions from the fundamental solution $\Phi(x, z)$ as it does for the Laplace equation (see, e.g., Ref. 8). Actually, the explicit form of the Dirichlet–Green's function G was derived in Ref. 16 when Ω is a central disk. But we could not find a convenient literature on the explicit form of the Neumann–Green's function G_N, and hence in the rest of this section, we shall give a brief derivation of the explicit forms of both G_N and G when Ω is a central disk of radius R. Before this, we would like to note that there are some useful identities of Green's functions established in Ref. 8 for general shaped domains.

We first recall the fundamental solution $\Phi(x, z) = \frac{i}{4}H_0^{(1)}(k|x - z|)$ associated with the Helmholtz operator $-\Delta - k^2$ and its special representation (cf. Ref. 15):

$$\Phi(x, z) = \frac{i}{4}\sum_{n=-\infty}^{\infty} J_n(k|z|)H_n^{(1)}(k|x|)e^{in(\phi-\phi')}, \tag{57}$$

where $|x| > |z|$ and $x = |x|e^{i\phi}$, $z = |z|e^{i\phi'}$ in polar coordinates. Here $H_n^{(1)}(t)$ is the first kind of Hankel functions of order n. Noting that $G_N(x, z) = \Phi(x, z) - u(x, z)$, where $u(x, z)$ solves (49). Now we write $u(x, z)$ as

$$u(x, z) = \sum_{n=-\infty}^{\infty} a_n J_n(k|x|)e^{in\phi}. \tag{58}$$

By direct computations using the boundary condition in (49) and the representation (57) we obtain

$$a_n = \frac{i H_n^{(1)'}(kR)J_n(k|z|)e^{-in\phi'}}{4J_n'(kR)}. \tag{59}$$

Next, we show that $u(x, z)$ in (58) with the corresponding coefficients given by (59) is well-defined in $H^1(\Omega)$. Using the following asymptotic behaviors of $J_n(t)$ and $H_n(t)$ for fixed t and sufficiently large n (cf. Ref. 1),

$$J_n(t) \sim \frac{1}{\sqrt{2\pi n}} \cdot (\frac{et}{2n})^n, \quad H_n^{(1)}(t) \sim -i\frac{\sqrt{2}}{\sqrt{\pi n}} \cdot (\frac{2n}{et})^n, \tag{60}$$

and the relation $J_n'(t) = \frac{1}{2}(J_{n-1}(t) - J_{n+1}(t))$, $H_n^{(1)'}(t) = \frac{1}{2}(H_{n-1}^{(1)}(t) - H_{n+1}^{(1)}(t))$, one can verify that $|a_n J_n(k|x|)| \sim \frac{1}{n\pi} \cdot (\frac{|z|}{R})^n \cdot (\frac{|x|}{R})^n$, $a_n J_n'(k|x|) \sim \frac{2}{\pi kR} \cdot (\frac{|z|}{R})^n \cdot (\frac{|x|}{R})^{n-1}$. By further using these asymptotic results, it is straightforward to show that $\sum_{n=-N}^{N} a_n J_n(k|x|)e^{in\phi}$ converges to $u(x, z)$ in $H^1(\Omega)$ as $N \to \infty$. Hence, the Neumann–Green's function $G_N(x, z)$ is given by

$$G_N(x, z) = \Phi(x, z) - \sum_{n=-\infty}^{\infty} \frac{i H_n^{(1)'}(kR)J_n(k|z|)e^{-in\phi'}}{4J_n'(kR)} J_n(k|x|)e^{in\phi}, \tag{61}$$

for $|x| > |z|$ and $x = |x|e^{i\phi}$, $z = |z|e^{i\phi'}$.

In a similar manner, one can find $G(x, z)$ by solving (30) that

$$G(x, z) = \Phi(x, y) - \sum_{n=-\infty}^{\infty} \frac{i H_n^{(1)}(kR)J_n(k|z|)e^{-in\phi'}}{4J_n(kR)} J_n(k|x|)e^{in\phi}, \tag{62}$$

for $|x| > |z|$ and $x = |x|e^{i\phi}$, $z = |z|e^{i\phi'}$.

V. NUMERICAL EXPERIMENTS AND DISCUSSIONS

In this section, we present some numerical experiments to illustrate the strength of our proposed sampling approach developed in Secs. II–IV. For simulation, we choose both the surrounding medium Ω and the test domain $\widetilde{\Omega}$ as a disk centered at (0, 0) with radius $R = 5.5$ in $\mathbb{R}^2$.

We first list some crucial parameters to be used: k for the wave number, δ for the noise level, $d = (d_x, d_y)^T$ for unitary incident direction, and $c = (c_x, c_y)^T$ for the object shifting with displacements c_x and c_y from the origin.

We shall test five different scatterers for systems (1) and (2): a unit disk, a kite, a crack, and a flower-shape scatterer which are denoted by **B**, **K**, **C**, and **F**, respectively, and a combination of **B** and **K** (at different locations). These scatterers can be parameterized as follows:

$$\texttt{Ball:} \qquad \mathbf{x}(t) = (\cos t, \sin t)^T, \quad 0 \le t \le 2\pi, \tag{63}$$

$$\texttt{Kite:} \qquad \mathbf{x}(t) = (\cos t + 0.65\cos 2t - 0.65, 1.5\sin t)^T, \quad 0 \le t \le 2\pi. \tag{64}$$

$$\texttt{Crack:} \qquad \mathbf{x}(t) = (t, t)^T, \quad -1 \le t \le 1, \tag{65}$$

$$\texttt{Flower:} \qquad \mathbf{x}(t) = ((1 + 0.2\sin 6t)\cos(t), (1 + 0.2\sin 6t)\sin(t))^T, \quad 0 \le t \le 2\pi. \tag{66}$$

The synthetic near-field data are generated by solving the Helmholtz equation of the direct problem corresponding to the systems (1) and (2) with isoparametric quadratic finite elements. We solve the discrete system over a family of increasingly finer meshes over the computational domain $\Omega \setminus \overline{D}$ until the relative error is small, i.e., less than 10^{-3}, which, compared with the noise level we added, is negligible and viewed as noise-free.

The synthetic near-field data along the medium boundary Γ are then subjected pointwise to uniform random noise, in magnitude as well as in direction, added according to the following formula:

$$U = U + \delta\, r_1 |U| \exp(i\pi\, r_2)\,, \tag{67}$$

where U may be the measurement data from u or $\frac{\partial u}{\partial \nu}$, r_1 and r_2 are two uniform random numbers, both ranging from -1 to 1, and δ represents the noise level. For each mesh point z, the corresponding integral equation is discretized through the mid-point quadrature rule at the equidistant points on the test boundary $\partial\widetilde{\Omega}$. It is noted that the integral kernel is quite smooth and thus the resulting matrix after discretization is highly ill-posed with its condition number ranging from 10^{16} to 10^{18}. Hence certain regularization in solving the discrete system is necessary. In all our test, the linear system is solved by using the Tikhonov regularization technique, with the corresponding regularization parameters determined by the Morozov discrepancy principle.

The measurement data depend on two variables: the observation location x on the medium boundary Γ and the incident direction d from the unit circle in $\mathbb{R}^2$, where we write $x = (R\cos(\phi), R\sin(\phi))^T$ with $\phi \in [-\pi, \pi]$, and $d = (\cos(\theta), \sin(\theta))^T$ with $\theta \in [-\pi, \pi]$. We compute the near-field measurement data at 100 equidistantly distributed observation points $x_j = (R\cos\phi_j, R\sin\phi_j)^T$, $\phi_j = 2j\pi/100 - \pi$, $j = 1, 2, \ldots, 100$, corresponding to 100 equidistantly distributed incident directions $d_j = (\cos\theta_j, \sin\theta_j)^T$, $\theta_j = 2j\pi/100 - \pi$, $j = 1, 2, \ldots, 100$. We may identify the observation points and incident directions with the index sequence $\{1, 2, \ldots, 100\}$ and illustrate the measurement data by the contour plots of the corresponding 100×100 matrices as shown in the following examples. Hereafter, the norms of the indicator function g_z and the residual of the integral equation $G_N(x, z) - Sg_z$ in the NtD case (or $\frac{\partial G(x,z)}{\partial \nu(x)} - Lg_z$ in the DtN case) are denoted by *g-norm* and the *res-norm*, respectively. Furthermore, these norms are plotted by transformation via 10-based logarithm for better visualization.

In the examples below, we always show in three columns, the contour plots of g-norm (left column) and res-norm (middle column) indicators, and two level sets (right column) with selected cut-off values compared with the true shapes. In the last column, the exact shape is plotted in red. The level set based on the g-norm indicator is plotted in black, while the other based on the res-norm one in blue, with the associated cut-off values attached to the curves. *From our proposed algorithms, the interior region of the reconstructed scatterer should be understood as the intersection of the interior parts enclosed by the respective blue and black curves.*

Example 1: Unit disk obstacle **B** with displacement $c = (-1.5, -1.5)^T$.

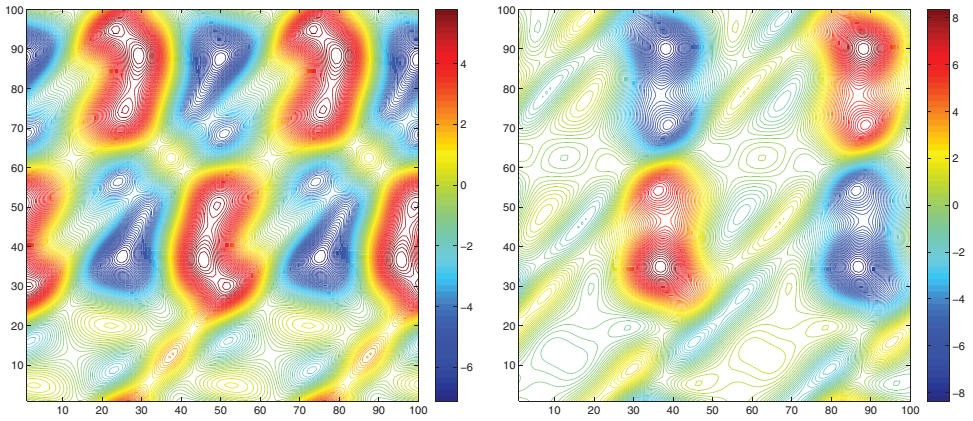

FIG. 1. Sample plots of the real (left) and imaginary (right) parts of the observation data.

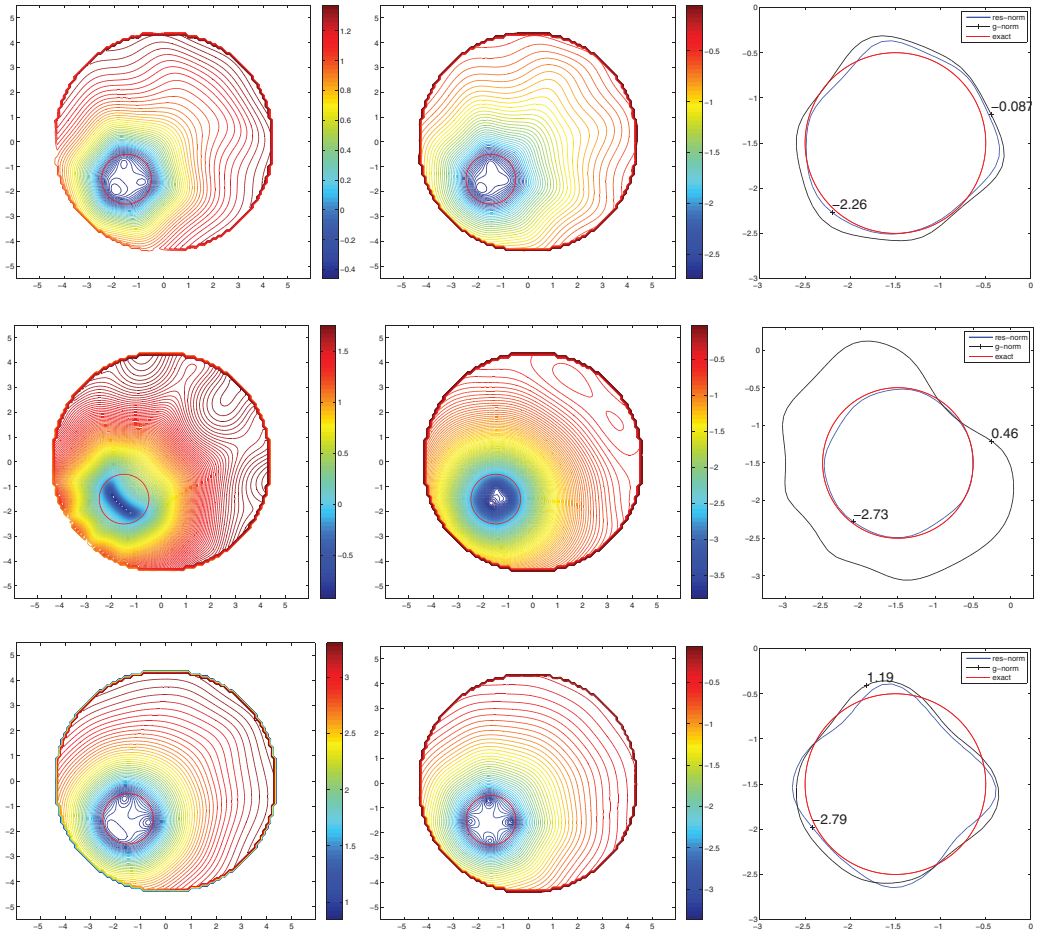

FIG. 2. Reconstruction tests in Example V. (First row) Plane incident wave of wave number $k = 1$ with the NtD map. (Second row) Plane incident wave of wave number $k = 1$ with the DtN map. (Third row) Cylindrical incident wave of order $\nu = 1$ with the NtD map.

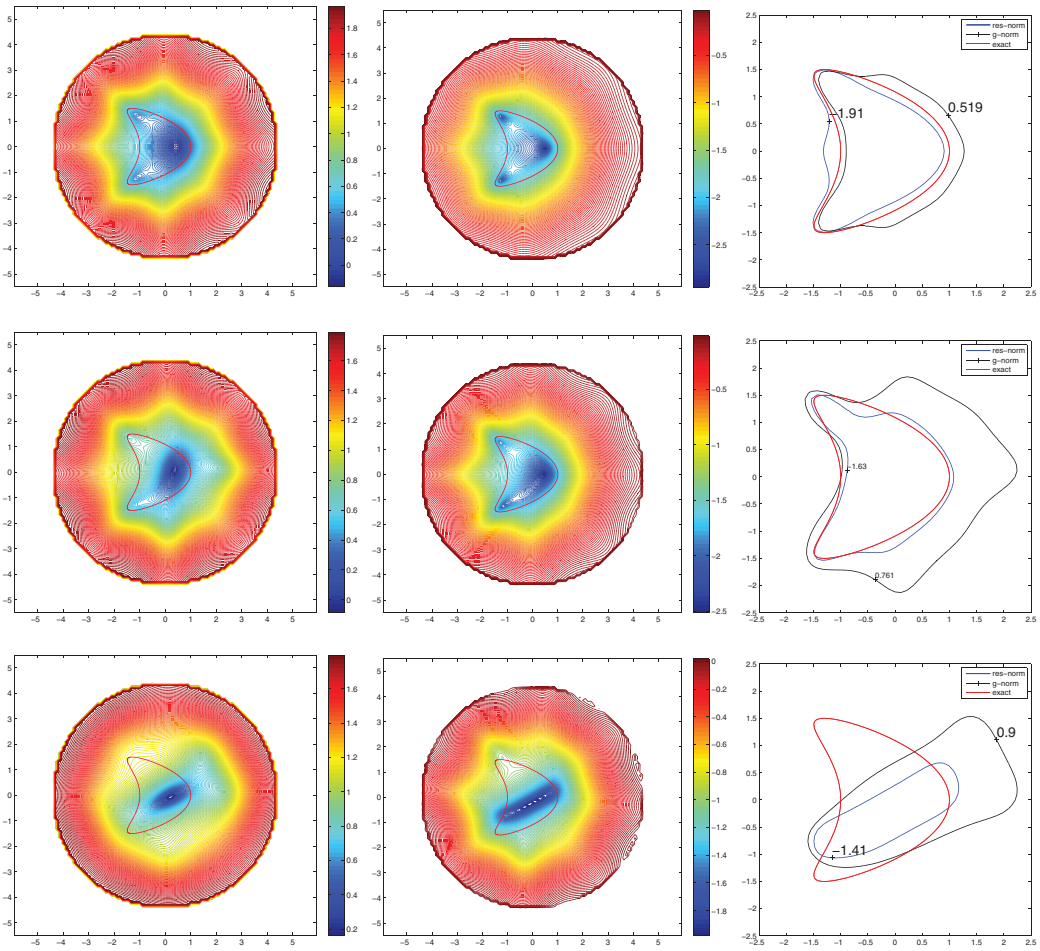

FIG. 3. Reconstruction tests in Example 2 with data measured with full aperture (Row 1), lower half aperture (Row 2), quarter aperture in the fourth quadrant (Row 3).

For illustration, we show in Figure 1 the contour plots of a sample near-field measurement data u with no noise when employing the plane incident wave with $k = 1$ and the NtD map, namely, injecting the Neumann data to generate synthetic boundary potential u. Except very few clues like self-similar patterns and periodicity, it is very hard to envisage the shape of the obstacle. The inverse problem we are confronted with is to reconstruct the unknown scatterer D from those elusive plots.

In Figure 2, we presents in three rows the reconstruction tests for different combinations of types of incident waves and measurement data. The noise level is fixed with $\delta = 0.01$ when using the NtD map. We add no noise for the test with the DtN map to avoid instability since the computation of measured Neumann data on the boundary are performed numerically by differentiating locally the computed potential.

By our proposed linear sampling method (LSM), it clearly shows in Figure 2 that the reconstructed shapes approximate well the actual disk. It is remarked that since the Tikhonov regularization and the Morozov discrepancy principle has been used, the g-norm and the res-norm indicators are related and this is reflected from the similar patterns of contour plots in Columns 1 and 2 of Figure 2. However, the difference of minutes of contour plots is still observable. In Row 2 of Figure 2, using the DtN map, we see that the location of the scatterer is well captured by the g-norm indicator, but the shape determined solely by the g-norm indicator is severely distorted compared with the exact one. This observation consolidates our prediction in Remark 2.8. Next, by further examining the

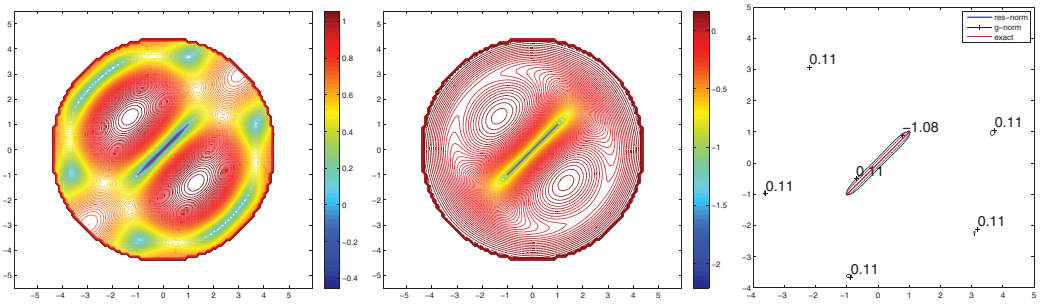

FIG. 4. Reconstruction test in Example 3.

suspicious region using the res-norm indicator, we can successfully rule out some other part where g-norm does not blow up and recover the fine details of the disk. To put simply, it is more sound to use two indicators for reconstruction in case that the g-norm indicator fails.

We remark that in our numerical experiment the wavelength is larger than the size of the target obstacle. For extended targets with more complex geometry, one may combine our method with some existing techniques, e.g., the multiscale technique developed in Ref. 4, to extract finer details of the targets by using multi-frequency measurements.

Example 2: Kite obstacle **K**.

In this example, we test a non-convex kite-shape scatterer by injecting cylindrical incident wave of order $\nu = 3$ and use the NtD map with noise level $\delta = 0.01$.

For this kite example, we investigate the possibility of using limited data for reconstruction. We gradually reduce incident angle from (i) full aperture $\theta \in [-\pi, \pi]$ to (ii) a half aperture in the lower half plane $\theta \in [-\pi, 0]$, and further to (iii) a quarter aperture in the fourth quadrant $\theta \in [-\pi/2, 0]$. In case (ii), the reconstructed object significantly lacks to symmetry as opposed to that from case (i). More precisely, we see in Row 2 of Figure 3 that the lower wing of the kite is better reconstructed than its upper one. When the incident angle is further restricted to a quarter aperture, Figure 3 tells us that only the rough location of the kite and the lower part facing the incident angles can be reasonably obtained.

Example 3: Crack obstacle **C**.

We try to detect an unknown crack buried in the medium. As is well known, imaging scatterers of thin type is quite challenging and has much interest in many practical applications (cf. Ref. 9). Cylindrical incident wave $\nu = 3$ combined with the NtD map is used with noise level $\delta = 0.02$. In Figure 4, the reconstruction based on the g-norm indicator has some outliers, which can be effectively eliminated by the res-norm indicator.

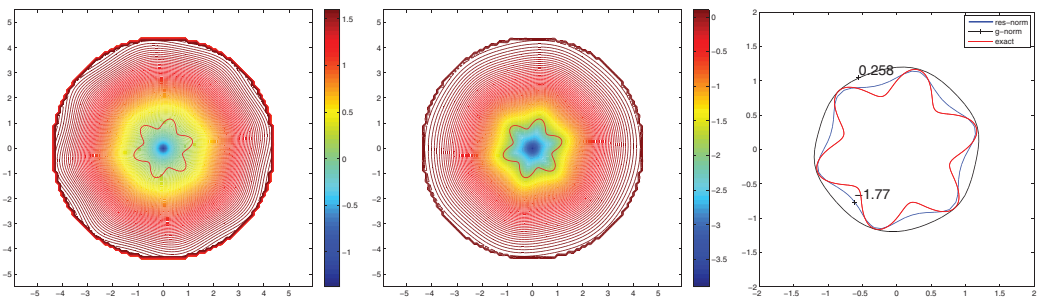

FIG. 5. Reconstruction test in Example 4.

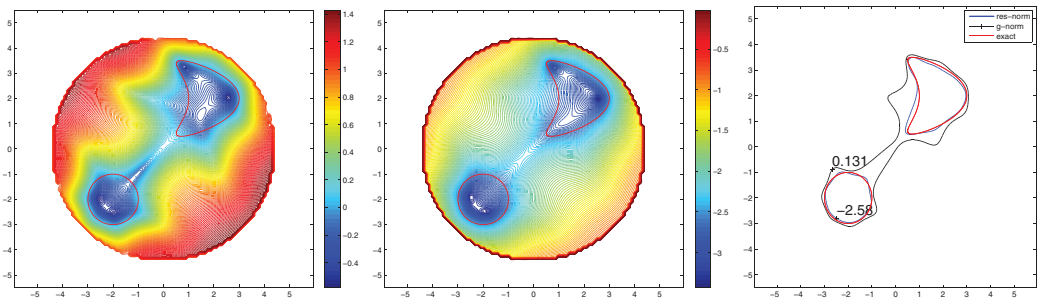

FIG. 6. Reconstruction test in Example 5.

Example 4: Flower obstacle **F**.

We try to reconstruct a six-pedal flower, i.e., an extended object with fine structure on the boundary (cf. Ref. 3). Except the noise level $\delta = 0.05$, we adopt the same setting as in Example 3. As can be observed in Figure 5, the reconstructed shape based on the g-norm indicator can locate the rough location but with poor boundary characterization, while the res-norm indicator can improve the fine details to some extent and yields better reconstruction by showing more oscillation on the boundary.

Example 5: A combination of ball **B** and kite **K** obstacles with displacement $c_{ball} = (-2, -2)$ and $c_{kite} = (2, 2)^T$.

In this example, we test the multi-component obstacle scattering case with a combination of a unit ball **B** centered at $(-2, -2)^T$ and a kite **K** with some displacement at $(2, 2)^T$. Here the plane incident wave of wave number $k = 1$ with the NtD map is used with noise level $\delta = 0.01$. Due to strong multi-scattering interaction, we see in Figure 6, those parts of the identified objects facing each other are attracted to a certain degree based solely on the g-norm indicator, which cannot separate the components correctly. Aided with the res-norm indicator, we see that the two components are successfully separated and their boundaries are recovered much better than those by the g-norm solely.

VI. CONCLUDING REMARKS

In this work, we have developed a linear sampling-type method for the inverse obstacle scattering problem using near-fields through the DtN or NtD maps with planar or cylindrical incident waves. The method is mathematically justified, and numerical experiments are also presented to demonstrate the effectiveness of the method. We emphasize that the proposed method is basically for qualitative reconstructions, although we observe from our numerical experiments that some fine aspects of the underlying obstacles may be captured. However, the method is rather robust with respect to noise. We would like to mention the interesting work[5] for a related study on the resolution and stability analysis for the EIT problem. Finally, we make an interesting remark on the extreme case when the boundary on which the measurements are taken goes to infinity. One can easily come to a reconstruction method using the far-field data by some straightforward analysis and taking $x \to \infty$ in Eq. (5) or (8) which defines the indicator function g. Indeed, if one takes the inputs to be the plane waves, Eq. (8) will reduce to the original linear sampling method in the infinity case, and we refer to Refs. 11 and 29 and references therein for extensive numerical results for comparisons. However, as we emphasized in the Introduction, the indicator function in our proposed scheme exhibits different behaviors from those indicator functions in the original linear sampling method due to the distinct mapping properties of the boundary operators involved here.

ACKNOWLEDGMENTS

The authors are very grateful to the anonymous referee for the helpful suggestions and comments which significantly improve the manuscript. The work of Hongyu Liu is supported by NSF grant, DMS 1207784. The work of Jun Zou was substantially supported by Hong Kong RGC grants (Projects 405110 and 404611).

[1] Abramowitz, M. and Stegun, I. A., *Handbook of Mathematical Functions* (Dover, New York, 1965).
[2] Ammari, H., *An Introduction to Mathematics of Emerging Biomedical Imaging*, Mathematics and Applications Vol. **62** (Springer-Verlag, Berlin, 2008).
[3] Ammari, H., Beretta, E., Francini, E., Kang, H., and Lim, M., "Optimization algorithm for reconstructing interface changes of a conductivity inclusion from modal measurements," Math. Comput. **79**, 1757–1777 (2010).
[4] Ammari, H., Garnier, J., Kang, H., Lim, M., and Solna, K., "Multistatic imaging of extended targets," SIAM J. Imaging Sci. **5**, 564–600 (2012).
[5] Ammari, H., Garnier, J., and Solna, K., "Resolution and stability analysis in full-aperture, linearized conductivity and wave imaging," Proc. Am. Math. Soc. (in press).
[6] Ammari, H., Griesmaier, R., and Hanke, M., "Identification of small inhomogeneities: Asymptotic factorization," Math. Comput. **76**, 1425–1448 (2007).
[7] Ammari, H. and Kang, H., *Expansion Methods, Handbook of Mathematical Methods in Imaging*, Vol 1 (Springer-Verlag, New York, 2011), pp. 447–499.
[8] Ammari, H. and Kang, H., *Reconstruction of Small Inhomogeneities from Boundary Measurements* (Springer-Verlag, Berlin, 2004).
[9] Ammari, H., Kang, H., Lee, H., and Park, W. K., "Asymptotic imaging of perfectly conducting cracks," SIAM J. Sci. Comput. (USA) **32**, 894–922 (2010).
[10] Arens, T., "Why the linear sampling method works," Inverse Problems **20**, 163–173 (2004).
[11] Cakoni, F. and Colton, D., *Qualitative Methods in Inverse Scattering Theory* (Springer, 2006).
[12] Cavicchi, T. J. and O'Brien, W. D., Jr., "Acoustic scattering of an incident cylindrical wave by an infinite circular cylinder," IEEE Trans. Ultrason. Ferroelectr. Freq. Control **35**, 78–80 (1988).
[13] Chen, Y., "Inverse scattering via skin effect," Inverse Problem **13**, 647–667 (1997).
[14] Cheney, M., "The linear sampling method and the MUSIC algorithm," Inverse Problems **17**, 591–595 (2001).
[15] Chew, W. C., *Waves and Fields in Inhomogeneous Media* (Van Nostrand Reinhold, 1990).
[16] Chew, W. C., Jin, J. M., and Michielssen, E., "Complex coordinate stretching as a generalized absorbing boundary condition," Microw. Opt. Technol. Lett. **15**, 363–369 (1997).
[17] Colton, D. and Haddar, H., "An application of the reciprocity gap functional to inverse scattering theory," Inverse Problems **21**(1), 383–398 (2005).
[18] Colton, D. and Kirsch, A., "A simple method for solving inverse scattering problems in the resonance region," Inverse Problems **12**, 383–393 (1996).
[19] Colton, D. and Kress, R., *Inverse Acoustic and Electromagnetic Scattering Theory*, 2nd ed. (Springer-Verlag, New York, 1998).
[20] Colton, D. and Kress, R., "Using fundamental solutions in inverse scattering," Inverse Problems **22**, R49 (2006).
[21] Colton, D. and Monk, P., "A linear sampling method for the detection of leukemia using microwaves," SIAM J. Appl. Math. **58**, 926–941 (1998).
[22] Gebauer, B., Hanke, M., Kirsch, A., Muniz, W., and Schneider, C., "A sampling method for detecting buried objects using electromagnetic scattering," Inverse Problems **21**, 2035–2050 (2005).
[23] Gilbarg, D. and Trudinger, N. S., *Elliptic Partial Differential Equations of Second Order* (Springer, 2001).
[24] Ide, T., Isozaki, H., Nakata, S., Siltanen, S., and Uhlmann, G., "Probing for electrical inclusions with complex spherical waves," Commun. Pure Appl. Math. **60**, 1415–1442 (2007).
[25] Ikehata, M. and Itou, H., "Extracting the support function of a cavity in an isotropic elastic body from a single set of boundary data," Inverse Problems **25**, 105005 (2009).
[26] Ikehata, M., "Enclosing a polygonal cavity in a two-dimensional bounded domain from Cauchy data," Inverse Problems **15**, 1231–1241 (1999).
[27] Ikehata, M., "How to draw a picture of an unknown inclusion from boundary measurements. Two mathematical inversion algorithms," J. Inv. Ill-Posed Problems **7**, 255–271 (1999).
[28] Isakov, V., *Inverse Problems for Partial Differential Equations*, 2nd ed. (Springer, New York, 2006).
[29] Kirsch, A. and Grinberg, N., *The Factorization Method for Inverse Problems* (Oxford University Press, 2008).
[30] Li, J. Z., Liu, H. Y., and Zou, J., "Multilevel linear sampling method for inverse scattering problems," SIAM J. Sci. Comput. (USA) **30**, 1228–1250 (2008).
[31] Li, J. Z., Liu, H. Y., and Zou, J., "Strengthened linear sampling method with a reference ball," SIAM J. Sci. Comput. (USA) **31**, 4013–4040 (2009).
[32] McLean, W., *Strongly Elliptic Systems and Boundary Integral Equations* (Cambridge University Press, 2000).
[33] Nakamura, G. and Yoshida, K., "Identification of a non-convex obstacle for acoustical scattering," J. Inv. Ill-Posed Problems **15**, 611–624 (2007).
[34] Potthast, R., *Point Sources and Multipoles in Inverse Scattering Theory*, Chapman & Hall/CRC Research Notes in Mathematics 427 (Chapman and Hall, 2001).

[35] Potthast, R., "A survey on sampling and probe methods for inverse problems," Inverse Problems **22**, R1 (2006).
[36] Uhlmann, G., "Visibility and invisibility," in *ICIAM 07-6th International Congress on Industrial and Applied Mathematics* (European Mathematical Society, Zürich, 2009), pp. 381–408.
[37] Uhlmann, G., "Electrical impedance tomography and Calderón's problem," Inverse Problems **25**, 123011 (2009).